Supplementary Material for Urban night sky is drastically lit up by a few decorative buildings: Natural experiments from Earth Hour

Chu Wing So[1,*], Chun Shing Jason Pun[1], Shengjie Liu[1,2], Sze Leung Cheung[3,4,5], Ho Keung Kenneith Hui[5], Kelly Blumenthal[4], and Constance E. Walker[6]

[*]socw@connect.hku.hk

ABSTRACT

Light pollution, an underappreciated environmental issue, has gained attention in recent years. While controlling light pollution requires sustained efforts, Earth Hour offers a unique natural experimental setting to assess temporary lights-out measures. Using photometric and spectroscopic sensors, we observed up to 50% night sky darkening during Earth Hour from 2011 to 2024 in Hong Kong, primarily as a result of a small but critical number of lights-out instances in central business districts, as evidenced by crowd-sourced photography records. Weekend nighttime activities in the city remained unaffected. The emission reductions mostly occurred in the 445–500, 500–540, and 615–650 nm spectral ranges—corresponding to peak emissions from LED billboard screens—and in the 585–595 nm range, associated with metal halide floodlights used for facades and billboards. Our study identifies these sources as major contributors to urban light pollution. By combining multi-modal observations, we offer a comprehensive assessment of light pollution sources and the potential benefits of sustainable lighting practices in urban environments. This research highlights the importance of targeted light pollution mitigation efforts and provides critical insights for policymakers to enhance urban sustainability and human well-being.

Supplementary Note 1: Illuminated billboard and facade as seen from all-sky images

After verifying through site visits and map checks, it was determined that the light sources labeled *b* and *d* in the all-sky images (see labels overlaid on Figure 4 in main text hereafter) correspond to two billboards located on separate buildings at different distances from the camera. The billboard to the north, labeled *b*, is situated on a hotel, while the one labeled *d* is mounted on a business tower in the background. These two billboards appear indistinguishable because they are aligned along nearly the same line of sight from the camera. Additionally, the sensor's pixels in that direction became saturated, causing blooming effects from the billboards' emissions. A similar situation occurs with light sources *h* and *i*, where the facade lighting of a skyscraper (*h*) visually merges with the billboard installed on a business tower (*i*).

Supplementary Note 2: Light patches as seen in all-sky images

Through site visits and analysis of all-sky images, it was confirmed that the light patches inside the yellow boxes 1 and 2 (see labels overlaid on Figure 4 in main text hereafter) are not actual light sources. The box 1 corresponds to the wall of a performance facility facing the hotel with the billboard *b*, while the box 2 corresponds to the glass-walled upper floor of a museum facing the hotel with a video wall *g*. Although these patches appeared to dim during the lights-out, they were actually reflections of the billboards *b* and the video wall *g*, respectively. These observations imply that the brightness of the billboards was sufficient to create strong reflections on nearby structures.

Supplementary Note 3: Lights-out participation as seen in all-sky images

We examined the lights-out participation on light sources observed in all-sky images among years and summarized the findings in Supplementary Tables 1 to 3. For instance, the facade light on the hotel *a* was only partially dimmed in 2015 and remained fully illuminated in 2020 and 2023, indicating limited participation. Similarly, the facade light *e* illuminated throughout the 2022 event, denoting a lack of participation from that location. Conversely, the facade light on hotel *c* did not turn on even before the Earth Hour event in 2021, suggesting it was already switched off prior to the campaign. Similarly, the facade light on the skyscraper *f* only turned on at 22:15 after the event in 2024, implying a longer duration of participation. Additionally, the behavior of outdoor billboards during Earth Hour was also heterogeneous. In 2022, the billboard on hotel *b* and the facade light on the same building *c* turned off earlier at 19:25 and turned back on later at 21:40, implying a longer duration

Table 1. Earth Hour participation as seen from all-sky images in 2015-2016. **on** indicates that the light remained on during Earth Hour, while **off** means that the light was turned off for Earth Hour.

label	building nature	light source	2015	2016
a	hotel	facade	partially off	off
b	hotel	billboard	not installed	not installed
c	hotel	facade	not installed	not installed
d	business tower	billboard	off	off
e	performance facility	facade	off	off
f	skyscraper	facade	under construction	under construction
g	hotel	video wall	off	off
h	skyscraper	facade	off	off
i	business tower	billboard	off	off

Table 2. Same as Supplementary Table 1, but for 2017-2021.

label	2017	2018	2019	2020	2021
a	off	off	off	on	off
b	not installed	not installed	not installed	off	off
c	not installed	not installed	not installed	off	remained off that evening
d	off	off	off	off	on/off alternatively
e	off	off	off	off	off
f	under construction	under construction	off	off	off
g	off	off	off	off	off
h	off	off	off	off	off
i	off	off	off	off	off

of participation. The billboard on business tower *d* alternated between being illuminated at lower intensity and completely turned off during the event in 2021. Furthermore, the all-sky imagery revealed the introduction of new lighting installations and building developments over the years. The billboard on hotel *b* and the facade light on the same building *c* were identified as new additions since 2020. Similarly, the skyscraper where the facade light *f* is located was still under construction in 2018, with the light only partially turning off before the building's completion in April of that year.

Supplementary Note 4: Impact of short-term cloud variations on NSB observations

NSB values are sensitive to cloud cover, and there is a strong correlation between cloudiness and NSB measurements. Although we were unable to quantitatively assess cloudiness, we calculated the standard deviation of NSB data (σ) from all available positive and negative datasets collected from TST (see Methods for the definitions of positive and negative datasets, see

Table 3. Same as Supplementary Table 1, but for 2022-2024.

label	2022	2023	2024
a	off	on	off
b	off 19:25-21:40	off <21:30	off
c	off 19:25-21:40	on	off
d	off	off	off
e	on	off	? (view blocked)
f	off	off 20:00-21:00	off 20:25-22:15
g	off	off	off
h	off	remained >20:30	off
i	off	off	off

Table 4. Cloud amount variations quantified by NSB data fluctuations in term of data standard deviation (σ). 2014 and 2017 NSB data are unavailable.

Year	Positive or negative year	Size of weighted σ	Cloud condition
2011	positive	11.8%	cloudy
2012	negative	17.6%	cloudy
2013	positive	7.2%	clear
2015	positive	5.9%	clear
2016	negative	19.8%	cloudy
2018	negative	21.6%	cloudy
2019	positive	12.9%	cloudy
2020	positive	12.1%	cloudy
2021 (>20:50)	positive	4.9%	clear
2022	positive	16.3%	cloudy
2023	positive	8.2%	cloudy
2024	negative	39.8%	cloudy

Supplementary Notes 9 to 11 for additional details) to quantify the variation in cloud cover during each Earth Hour. To exclude the effects of Earth Hour dimming, we focused on specific time windows: 20:00:00 to 20:24:59, 20:35:00 to 21:24:59 and 21:35:00 to 21:59:59. For the year 2021, we omitted data collected prior to 20:50, causing the first time window to be skipped and the second window to begin at 20:50. Supplementary Table 4 provides the sizes of σ relative to the average NSB in each time window, weighted by the number of data points.

Together with all-sky and wide-field camera observations, this approach allows us to identify the degree of variability associated with cloudiness[1]. Larger σ values indicate greater fluctuations in cloud amount, corresponding to a cloudier sky. Conversely, smaller σ values imply more stable conditions with less variability in cloud amount.

An important finding from the fluctuation analysis is that the years classified as positive correspond to smaller weighted σs. This suggests that when cloud variability during the Earth Hour evening was relatively low, Earth Hour impacts were more easily detected. Conversely, in years with larger weighted σ—referred to as negative years—the ability to observe the effects of Earth Hour was significantly diminished. This observation also clarifies why negative datasets exist, despite the event occurring annually.

In addition to calculating σ, we also evaluated other cloud variability indicators referenced in the literature[2,3]. Although these alternative methods provided similar assessments of cloudiness, the standard deviation approach aligned more effectively with our observations. This makes it the preferred method for quantifying cloud variability in our analysis.

Supplementary Note 5: Removing cloud influences from NSB observations during Earth Hour 2021

As shown in the all-sky images in Supplementary Figure 1, clouds affected some NSB observations in 2021. The original light curve is presented in Supplementary Figure 2. To estimate the impact of clouds, we refer to the all-sky images. Since the exposure times of the individual all-sky images were not recorded, we compared minutely averaged NSB values with the digital numbers (DN) around the zenith in the corresponding all-sky image taken within the same minute. The size of the zenith area was aligned with the sensitivity of the NSB sensor (see Supplementary Figure 4). As NSB values gradually changed, except during moments of lights-out and lights-on—we attributed any sudden significant change in DN between two images to a variation in the exposure time. Assuming a constant level of ALAN, we identified two periods (19:51-20:29 and 20:31-21:29) during which the camera's exposure time remained stable. We found a strong linear correlation between NSB and DN values during each of these periods, as illustrated in Supplementary Figure 5. Changes in DN values can be attributed to the presence of clouds. If we assume that aerosol and atmospheric conditions (aside from clouds) remain constant, the lowest DN value observed during this period can be considered the ideal cloudless DN value. When clouds are present, they increase the DN values. Thus, for each exposure-time-stable period, we can calculate the sky brightening change due to clouds (δ_{NSB}) based on the change in DN (δ_{DN}). This relationship can be expressed as:

$$\begin{aligned} \delta_{\mathrm{NSB}} &= a \times \delta_{\mathrm{DN}} \\ &= a \times (\mathrm{DN} - \mathrm{DN}_{\mathrm{min}}) \end{aligned} \tag{1}$$

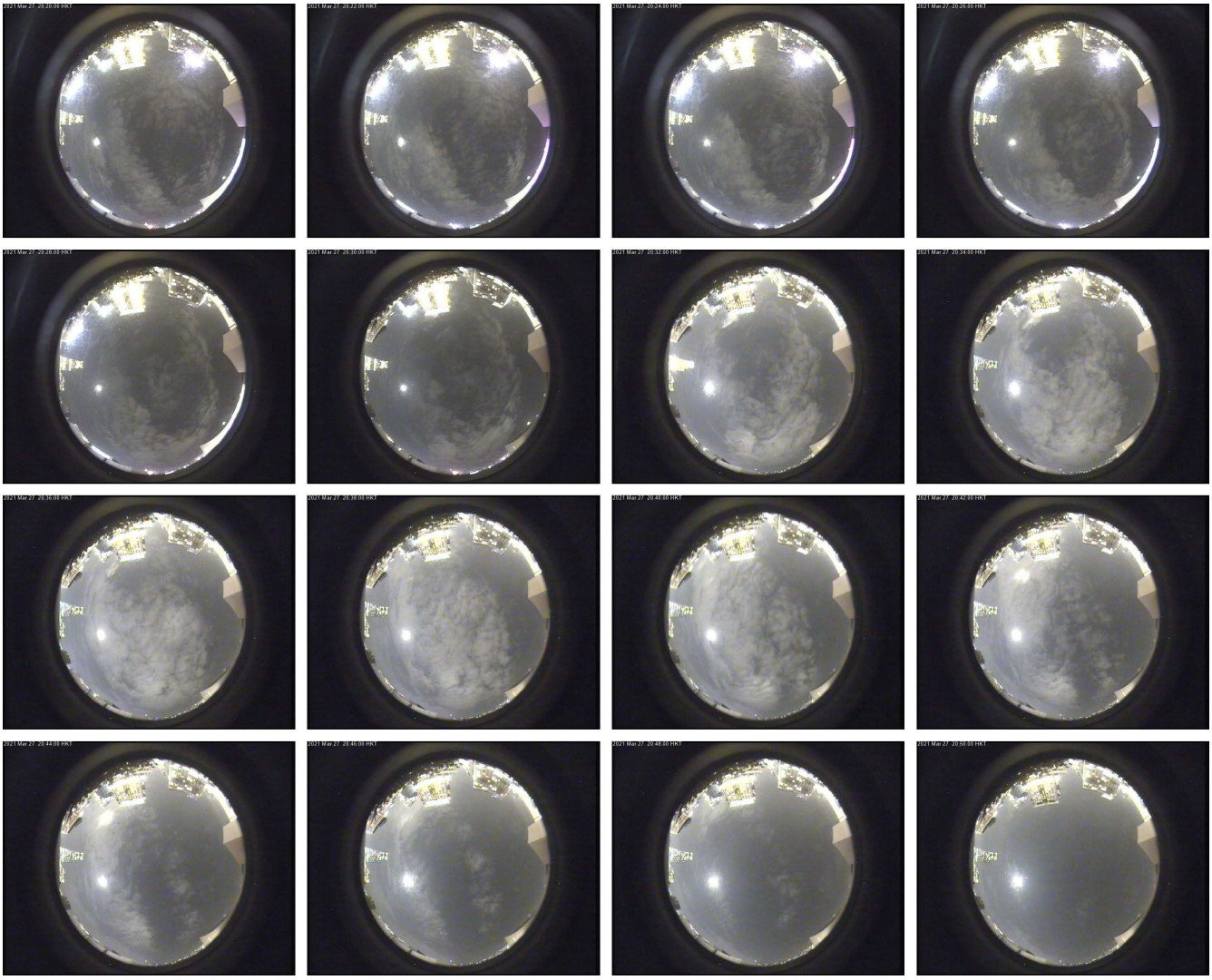

Figure 1. The image sequence, presented at 2-minute intervals from left to right and top to bottom, depicts the changing cloud conditions between 20:20 and 20:50 during Earth Hour 2021. The Moon appeared as a bright spot in the images. North is oriented at the top of the images. The all-sky images are courtesy of the Hong Kong Space Museum.

where a represents the slope derived from the linear regression between the values of NSB and DN. The term δ_{DN} is defined as the difference between the observed DN value and the minimum DN value ($\mathrm{DN}_{\mathrm{min}}$). In practice, we corrected the NSB values recorded during the time intervals of 20:00-20:30 and 20:31-20:49 using the slopes determined from the exposure-time-stable periods of 19:51-20:29 and 20:31-21:29, respectively. This correction allows for a more accurate representation of the NSB values by accounting for the effects of cloud cover during those specific time frames.

Supplementary Note 6: Changes in NSB observation configuration

Before July 2017, the SQM sensor for NSB observations was housed in a polycarbonate cuboid with a transparent cover to allow light to reach the sensor. In March 2012, we improved this setup by replacing a small portion of the cover with a circular glass piece, which served as a viewing window for better light transmission (see Ref.[4] for details). Since July 2017, a new design featuring a PVC tube housing has replaced the cuboid structure. A circular plate glass is attached to the top of the tube and acted as a viewing window. To minimize stray light from nearby sources, a light shield made of a black rubber sheet approximately 5 mm thick wraps around the tube. The upper edge of this shield is placed about 130 mm above the viewing window. The shield effectively blocks light incoming from zenith angles of about 30° to 40° and beyond, while keeping the sensor's zenith field of view ($\sim 20°$ in FWHM) unobstructed. Supplementary Figure 6 illustrates an example of this shielded configuration.

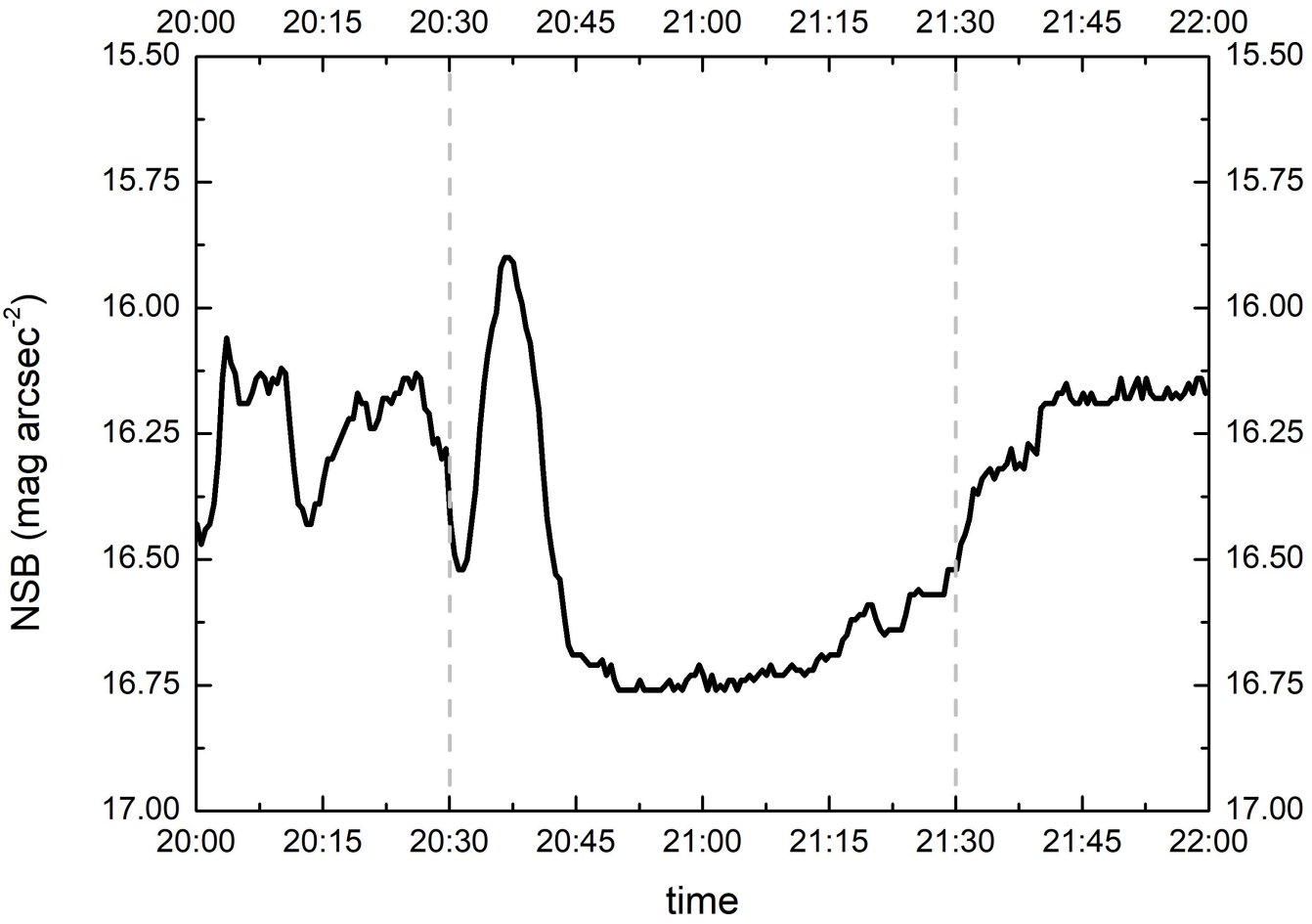

Figure 2. The original NSB light curve (in mag arcsec^{-2}) during Earth Hour 2021, showing different levels of cloud influence before and after 20:50. Vertical dashed lines mark the start and end of the lights-out period.

Compared to an unprotected sensor, both the glass window and the shielding reduce the amount of incoming skylight reaching the sensor. Additionally, prolonged exposure to sunlight has caused aging effects on both the sensor and the window[5,6]. Control experiments carried out in laboratory and field settings indicated that modifications to the viewing window and aging effects resulted in negligible offsets in the NSB measurements[4,7]. However, the application of the shielding darkened the measurements by 0.76 mag arcsec^{-2}.

In this study, we chose to ignore the effects of glass attenuation and sensor aging. Instead, we applied a +0.76 mag arcsec^{-2} offset to the raw NSB readings collected prior to the installation of the shield (i.e., before 2017) to correct for potential brightening caused by stray light from nearby sources. Nonetheless, our estimations of zenith sky darkening during the lights-out events each year remain unaffected by these factors, as we compared readings taken by the same device with the same configuration on the same evening.

Supplementary Note 7: Impact of atmospheric properties on NSB observations

The concentration of particulate matter, as well as the presence of fog or mist, can potentially influence observations[8,9]. However, no correlation has been found between particulate matter concentration and NSB measurements in Hong Kong[10]. Additionally, fog or mist were not present in our observations.

Supplementary Note 8: NSB data unit conversion and bandpass mismatch between SQM and *V*-band

The conversion from the logarithmic SQM readings (in mag arcsec^{-2}) to a linear quantity (in cd m^{-2}) followed Ref.[11]:

$$L = 10.8 \times 10^4 \times 10^{-0.4M}. \quad (2)$$

This approximation is imperfect because we assumed that the SQM's bandpass is equivalent to that of the Johnson astronomical photometric V-band[12]. There are alternative linearization methods to account for spectral discrepancies, one of which involves modeling the sensor's irradiance-to-frequency properties[13]. Unfortunately, we did not obtain the zero-point values for our sensors from the necessary calibrations for conversion. Instead, we utilized the published zero point values[13] to linearize M collected from 2017 onward, noting that older sensors may have undergone hardware and/or firmware changes that could invalidate the conversion. We then compared the results obtained from Supplementary Equation 2. Both conversion methods agreed within 1.5%. Given the small difference and the understanding that intra-night comparisons are adequate to detect the impacts of Earth Hour, the conversion derived from Supplementary Equation 2 is justified for this study.

Additionally, the spectral response of the SQM (240 nm FWHM) is broader than that of the broadband V-band filter (84 nm FWHM). Furthermore, their peak responses occur at slightly different wavelengths, with the SQM peaking at 540 nm and the V-band at 545 nm[12,14,15]. We have not corrected for this bandpass difference.

Supplementary Note 9: Visual inspection of NSB light curves

We visually inspected each NSB light curve to identify potential impacts from the Earth Hour lights-out. A total of eight TST datasets were classified as positive cases, and these are detailed in Supplementary Table 5, which includes observational details for each dataset.

In 2022, we observed a potential sky darkening around 20:30 at both the TBT (Tsim Bei Tsui) and MP (Mai Po Nature Reserve) stations, which have been operational since April and July 2021, respectively[4,16]. These stations are situated in the North District, close to Shenzhen, a modern metropolis connecting Hong Kong to mainland China. However, the anticipated sky brightening was not observed at these locations around 21:30. Further analysis is needed to determine whether the recorded sky darkening can be attributed to changes in the operation of light fixtures, such as Earth Hour participation, in Shenzhen.

Apart from TST, MP and TBT, negative cases were observed in locations outside of city centers. Detailed descriptions of each location can be found in previous studies[4,16]. We believe these cases are not false negatives due to the sensor's sensitivity, as SQMs can accurately capture variations as small as 10% (or 0.1 mag arcsec^{-2}) in very dark environments, such as national parks and dark sky sanctuaries[17,18]. However, we do not expect Earth Hour to have any measurable impact on the NSB at these remote locations, as the lights-out primarily involved buildings in city centers, a conclusion supported by a comprehensive survey conducted in 2021 (see Methods).

Supplementary Note 10: Non-linear fittings to NSB light curves

In addition to visual inspections, we performed non-linear curve fitting on all available datasets to objectively assess potential impacts from the Earth Hour lights-out. The fitting model used for this analysis is a Boltzmann step function, which allows us

Table 5. This table includes NSB observational details for candidate datasets that exhibit impacts from the lights-out during Earth Hour (i.e., positive cases). The last two columns indicate whether the datasets were accurately assessed through fittings. Additionally, lunar properties at 21:00 for each evening were calculated using ALCYONE EPHEMERIS version 4.3.

Year	Date in March	Lunar altitude	Lunar phase (if altitude>0)	20:00-22:00 sample size	20:30 fitting judged	21:30 fitting judged
2011	26	-56°		47	no	yes
2013	23	77°	0.84	120	yes	yes
2015	28	68°	0.62	240	yes	yes
2019	30	-81°		240	no	no
2020	28	11°	0.15	240	no	yes
2021	27	50°	0.98	240	no	yes
2022	26	-73°		240	no	no
2023	25	14°	0.17	240	yes	no

to capture the characteristic response of NSB values during the event:

$$y = \frac{M_1 - M_2}{1 + e^{(x-x_0)/dx}} + M_2 \tag{3}$$

where y is the NSB linear value converted by Supplementary Equation 2 measured at time x (converted to the number of minute after 19:30 that evening). The fitted parameters from the Boltzmann step function include x_0 (the turning time), dx (the rate of change at the turning point), M_1 and M_2 (the NSB readings before and after the turning point, respectively). A MATLAB (versions 9.9 R2020b and 9.11 R2021b) program was developed to perform the fittings using the *fit* function. The initial values for M_1 and M_2 were set to the average of the y values. The fittings covered data collected within $\pm$30 minutes of the lights-out at 20:30 (i.e., from 20:00:00 to 20:59:59, with the initial value of x_0 set to 60). This process was then repeated separately for the lights-on at 21:30 (i.e., from 21:00:00 to 21:59:59, with the initial value of x_0 set to 120).

The fittings produced a wide range of values for M_1, M_2, x_0 and dx. The positive data sets, as listed in Supplementary Table 5, met all of the following selection criteria at 20:30 or 21:30:

- Show a turning point within $\pm$5 minutes of the expected time (i.e., $55 \leq x_0 \leq 65$ or $115 \leq x_0 \leq 125$);
- Exhibit the expected change in sky brightness (i.e., $M_2 < M_1$ for 20:30 or $M_2 > M_1$ for 21:30); and
- Demonstrate a good fit between the model and the observed data (i.e., adjusted $R^2 \geq 0.9$).

Data and fittings for the positive cases are illustrated in Supplementary Figure 3. We also experimented with different sizes of fitting windows of $\pm$10 minutes and $\pm$60 minutes, and the same conclusions were reached in each case.

Supplementary Note 11: Compare visual inspection and non-linear fitting of NSB light curves

According to our definition, all visually-judged negative cases were also negative based on fittings, with one exception: the 2018 TST 21:30 case. Upon careful inspection of the light curve and the available all-sky images, it became clear that the cloud cover was gradually increasing from 21:00 (i.e., $M_2 > M_1$) and rapidly intensifying near 21:30 (i.e., $115 \leq x_0 \leq 125$). This led the fitting algorithm to interpret the cloud-induced NSB change at 21:30 as a positive case. Therefore, we classify this instance as a false positive, as the observed sky brightening was not related to the lights-out event.

The fitting process identified fewer positive cases than those detected by visual inspection, as indicated in Supplementary Table 5. Many of the fitting-negative cases were only slightly outside the expected ranges for adjusted R^2 or x_0. Additionally, the 2019 and 2022 TST cases at 20:30 and 21:30 were not classified as positive by the fitting method. However, careful examination of their light curves revealed noticeable impacts from Earth Hour, leading us to consider them marginal positive cases. Given that the fitting selection criteria are quite conservative and that human observations can often pick up patterns more effectively than machine algorithms, we combined the results from both methods to create a shortlist of candidate datasets for further analysis.

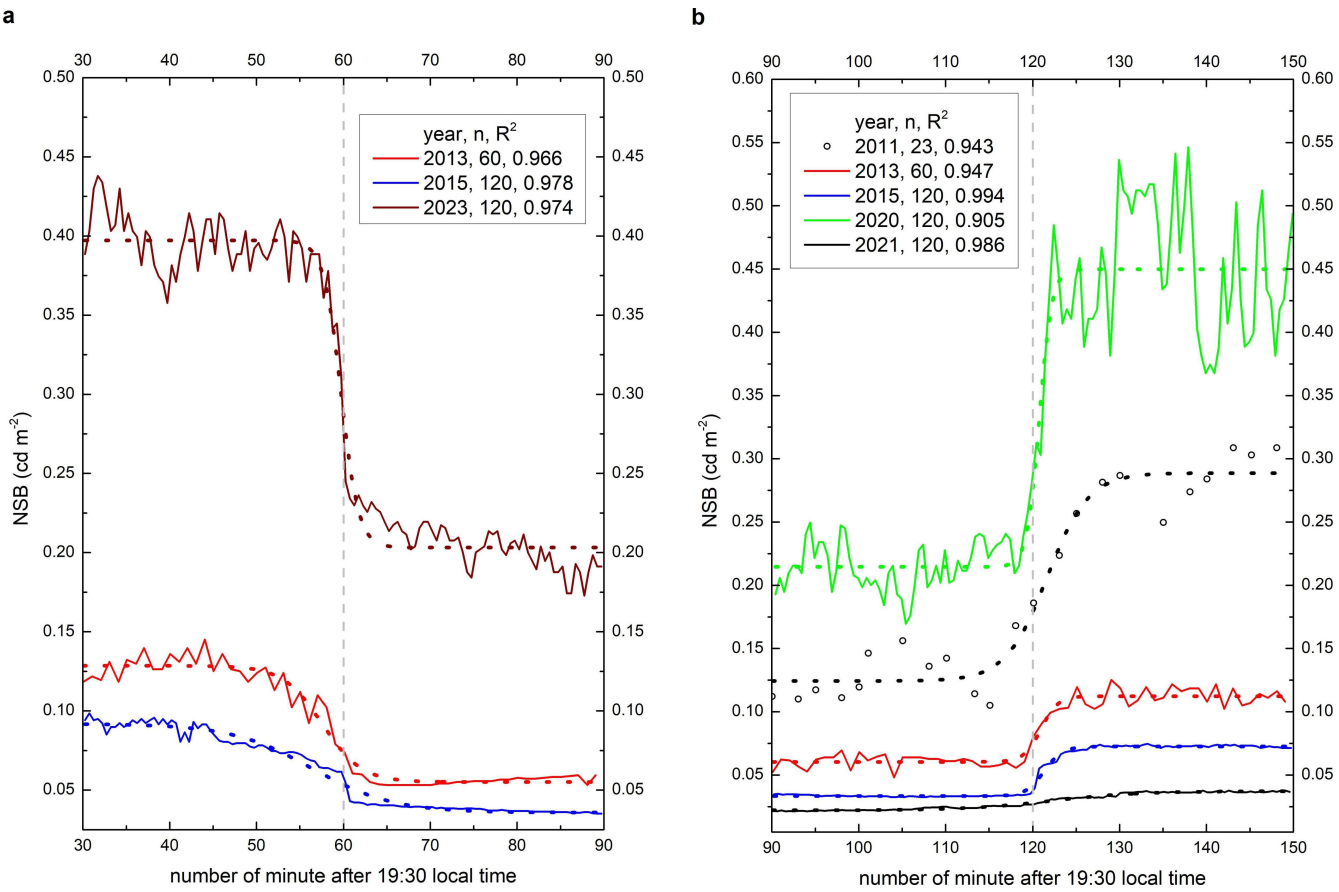

Figure 3. (**a**) The non-linear regression fittings for positive cases are displayed for the turnings at 20:30 (60 minutes after 19:30). (**b**) Same for 21:30 (120 minutes after 19:30). In the plots, solid curves represent the raw data converted to a linear scale using Supplementary Equation 2, while dotted curves indicate the best-fitted models. The light curve from 2011 is shown as circles to highlight its sparse temporal sampling resolution (150 seconds per data point) compared to the other datasets, which have sampling resolutions of either 60 or 30 seconds per data point. Vertical dashed lines indicate the start and end of the lights-out period. Significant F-test results from a One-Way ANOVA at a 5% alpha level reveal that all fittings have a P-value of 0. The legends indicate the lights-out year, sample size n and coefficient of determination R^2 for each year's fit.

Supplementary Note 12: Details of moonlight correction

In Equation 3 in Methods, B_{moon} is the theoretical Moon surface brightness in the unit of 10^{-9} cd m^{-2} defined as (see Ref.[4] for details):

$$B_{\text{moon}} = f(\phi_{\text{moon}}) \cdot 10^{-0.4kX(\phi_{\text{moon}})} \cdot 10^{-0.4(3.84+0.026|\alpha|+4\times10^{-9}\alpha^4)} \cdot \left[1 - 10^{-0.4kX(\phi)}\right], \tag{4}$$

where k is the extinction coefficient which depends on atmospheric optical properties and assumed to be 0.58 mag/airmass and α is the lunar phase angle. At the Moon's zenith angle ϕ_{moon} (in radian), $X(\phi)$ is the Moon's airmass $X(\phi_{\text{moon}}) = (1 - 0.96\sin^2\phi_{\text{moon}})^{-0.5}$. $f(\phi_{\text{moon}}) = f_{\text{Rayleigh}}(\phi_{\text{moon}}) + f_{Mie}(\phi_{\text{moon}})$ describes the moonlight Rayleigh and aerosols Mie scatterings:

$$f_{\text{Rayleigh}}(\phi_{\text{moon}}) = 10^{5.36} \cdot \left[1.06 + \cos^2\phi_{\text{moon}}\right], \tag{5}$$

$$f_{\text{Mie}} = 10^{6.15-\phi_{\text{moon}}/40} \tag{6}$$

if $\phi_{\text{moon}} \geq 10^\circ$, and

$$f_{\text{Mie}} = 6.2 \times 10^7 \cdot \phi_{\text{moon}}^{-2} \tag{7}$$

if $\phi_{\text{moon}} < 10^\circ$, where ϕ_{moon} in Supplementary Equations 6 and 7 are measured in degree.

References

1. Cavazzani, S. *et al.* Sky Quality Meter and satellite correlation for night cloud-cover analysis at astronomical sites. *Mon. Notices Royal Astron. Soc.* **493**, 2463–2471, DOI: 10.1093/mnras/staa416 (2020).
2. Ścieżor, T. The impact of clouds on the brightness of the night sky. *J. Quant. Spectrosc. & Radiat. Transf.* **247**, 106962, DOI: 10.1016/j.jqsrt.2020.106962 (2020).
3. Cereghetti, N., Strepparava, D., Bettini, A. & Ferrari, S. Analysis of light pollution in Ticino region during the period 2011-2016. *Sustain. Cities Soc.* **63**, 102456, DOI: 10.1016/j.scs.2020.102456 (2020).
4. So, C. W. *Observational Studies of Contributions of Artificial and Natural Light Factors to the Night Sky Brightness Measured through a Monitoring Network in Hong Kong*. Ph.D. thesis, The University of Hong Kong (2014). DOI: 10.5353/th_b5317025.
5. Fiorentin, P. *et al.* SQM ageing and atmospheric conditions: How do they affect the long-term trend of night sky brightness measurements. *Sensors* **25**, 516, DOI: 10.3390/s25020516 (2025).
6. Fiorentin, P. *et al.* Long-time trends in night sky brightness and ageing of SQM radiometers. *Remote. Sens.* **14**, 5787, DOI: 10.3390/rs14225787 (2022).
7. Bará, S. *et al.* Direct assessment of the sensitivity drift of SQM sensors installed outdoors. *Int. J. Sustain. Light.* **23**, 1–6, DOI: 10.26607/ijsl.v23i1.109 (2021).
8. Ścieżor, T. & Czaplicka, A. The impact of atmospheric aerosol particles on the brightness of the night sky. *J. Quant. Spectrosc. & Radiat. Transf.* **254**, 107168, DOI: j.jqsrt.2020.107168 (2020).
9. Ścieżor, T. & Kubala, M. Particulate matter as an amplifier for astronomical light pollution. *Mon. Notices Royal Astron. Soc.* **444**, 2487–2493, DOI: 10.1093/mnras/stu1577 (2014).
10. Pun, C. S. J. & So, C. W. Night-sky brightness monitoring in Hong Kong - a city-wide light pollution assessment. *Environ. Monit. Assess.* **184**, 2537, DOI: 10.1007/s10661-011-2136-1 (2012).
11. Andreas Hänela, T. P. *et al.* Measuring night sky brightness: methods and challenges. *J. Quant. Spectrosc. & Radiat. Transf.* **205**, 278–290, DOI: 10.1016/j.jqsrt.2017.09.008 (2018).
12. Bessell, M. S. Standard photometric systems. *Annu. Rev. Astron. Astrophys.* **43**, 293–336, DOI: 10.1146/annurev.astro.41.082801.100251 (2005).
13. Bará, S., Tapia, C. E. & Zamorano, J. Absolute radiometric calibration of TESS-W and SQM night sky brightness sensors. *Sensor* **19**, 1336, DOI: 10.3390/s19061336 (2019).

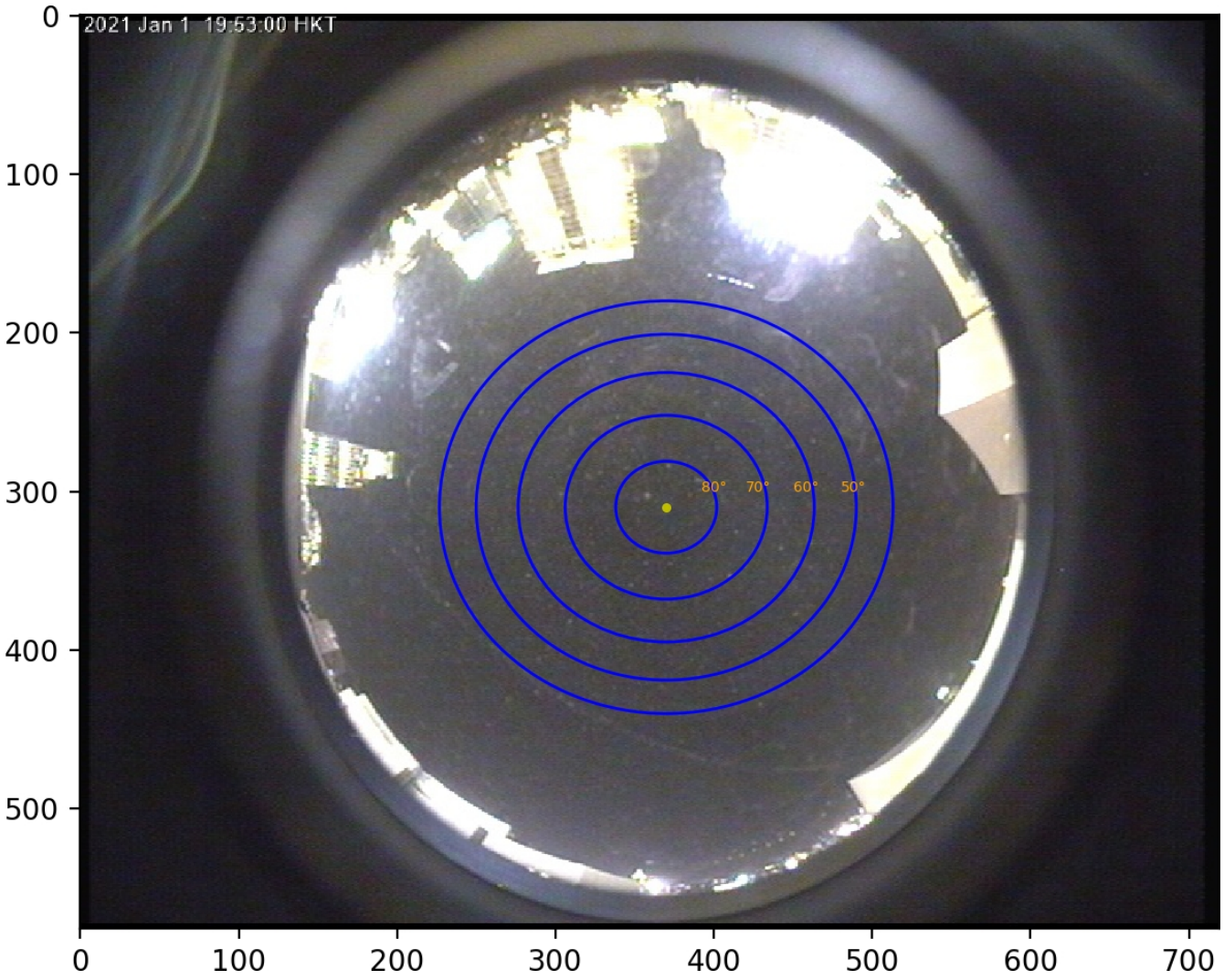

Figure 4. The contours represent the sky altitudes as observed from the all-sky camera. The innermost contour indicates the approximate area of the sky visible to the SQM. The yellow dot marks the zenith, located at the image coordinate $(x, y) = (370, 310)$. North is oriented at the top of each image. The all-sky image is courtesy of the Hong Kong Space Museum.

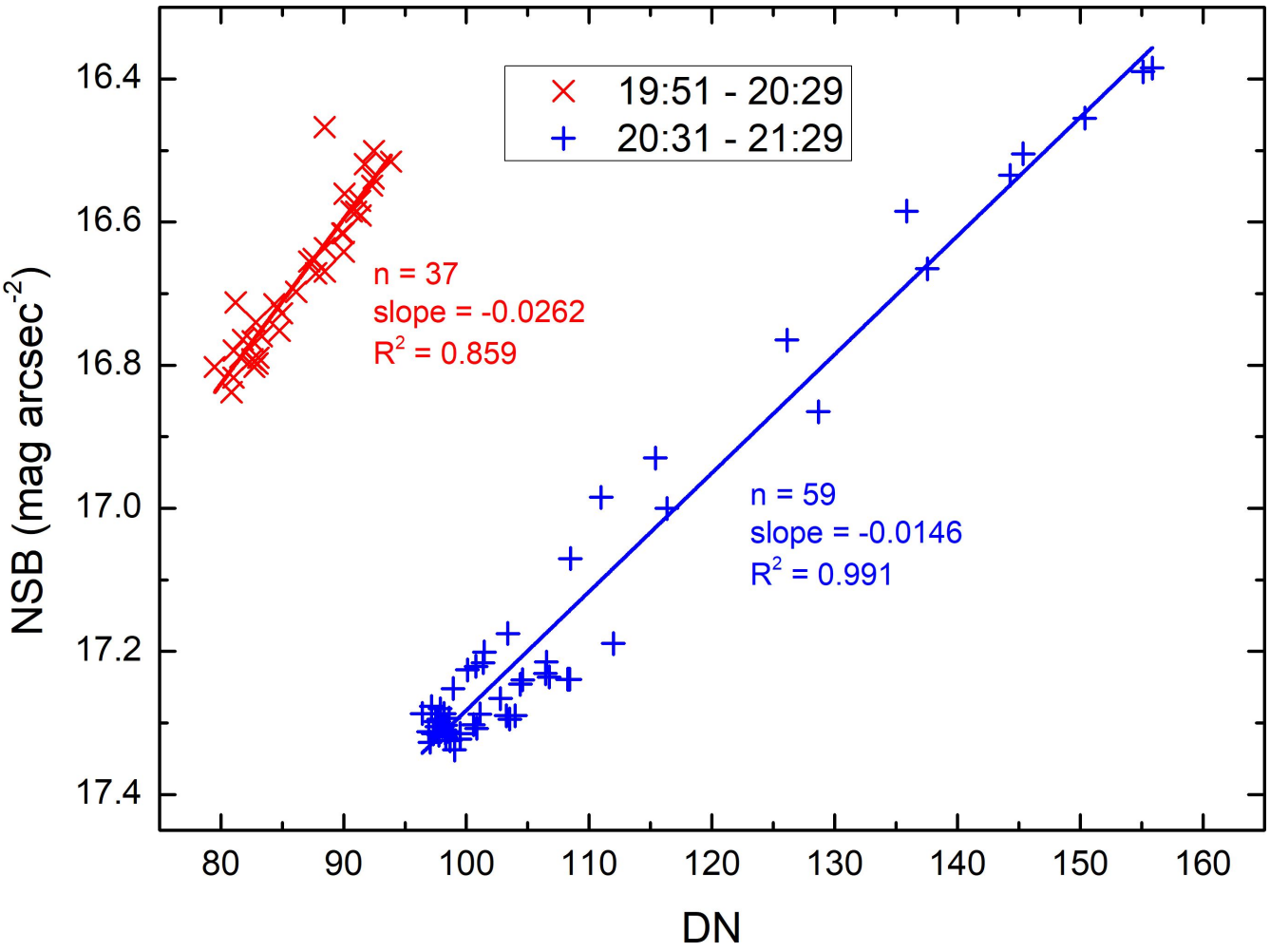

Figure 5. The correlations between the minutely averaged moonlight-corrected NSB and the digital numbers (DN) around the zenith on the all-sky image were analyzed during two selected periods in Earth Hour 2021. Significant F-test results from a One-Way ANOVA at a 5% alpha level reveal that both linear regression fittings have a P-value of 0. These correlations illustrate how changes in DN values correspond to variations in NSB, providing insights into the impact of cloud cover on sky brightness during the event.

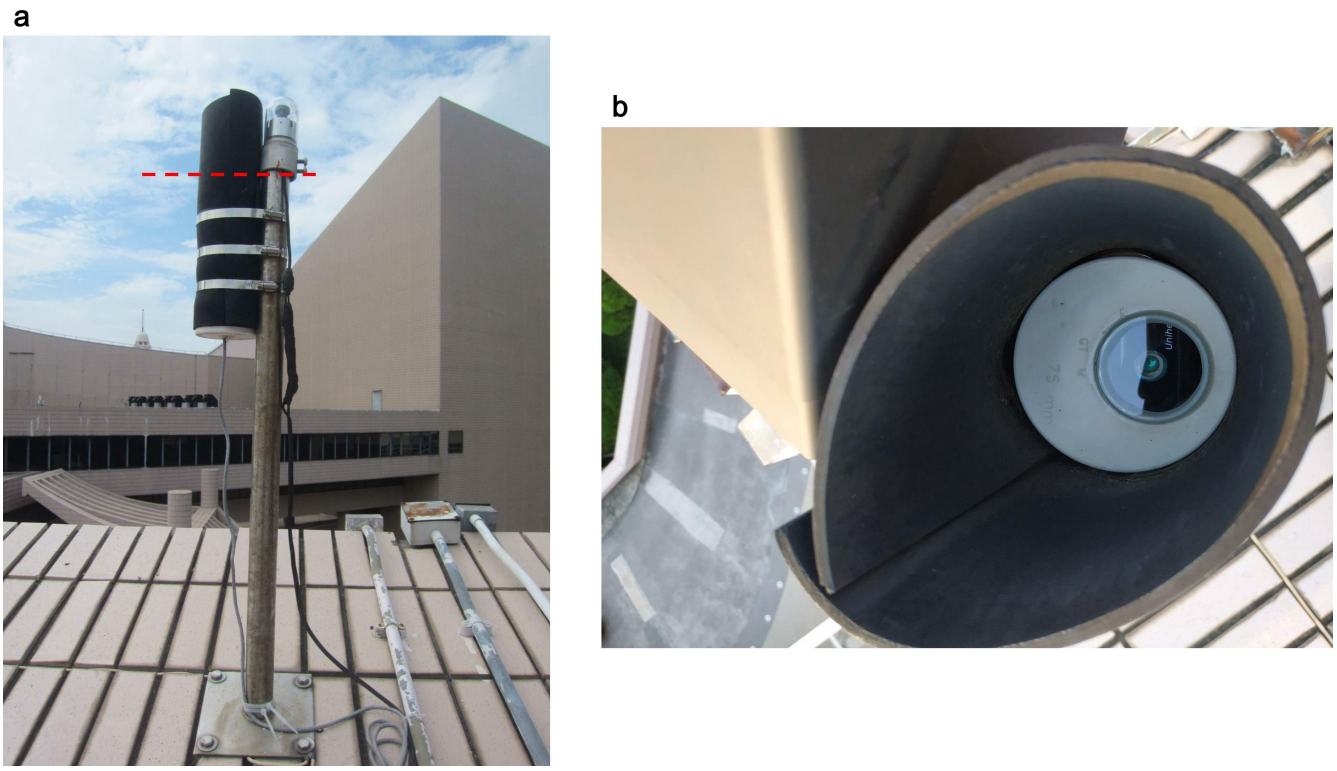

Figure 6. The SQM is housed within a white PVC tube, which is shielded by a black rubber sheet. (**a**) The red dashed line indicates the approximate level of the tube's top. (**b**) A top-down view, showcasing the glass window and the wrapped sensor. These photographs were taken in February 2019.

14. Barentine, J. C. Night sky brightness measurement, quality assessment and monitoring. *Nat. Astron.* **6**, 1120–1132, DOI: 10.1038/s41550-022-01756-2 (2022).

15. Cinzano, P. Night sky photometry with Sky Quality Meter. Tech. Rep., ISTIL Internal Report (2005).

16. Pun, C. S. J., So, C. W., Leung, W. Y. & Wong, C. F. Contributions of artificial lighting sources on light pollution in Hong Kong measured through a night sky brightness monitoring network. *J. Quant. Spectrosc. & Radiat. Transf.* **139**, 90, DOI: 10.1016/j.jqsrt.2013.12.014 (2014).

17. Grauer, A. D., Grauer, P. A., Davies, N. & Davies, G. Impact of space weather on the natural night sky. *Publ. Astron. Soc. Pac.* **131**, 114508, DOI: 10.1088/1538-3873/ab370d (2019).

18. Kolláth, Z. Measuring and modelling light pollution at the Zselic Starry Sky Park. *J. Physics: Conf. Ser.* **218**, 012001, DOI: 10.1088/1742-6596/218/1/012001 (2010).

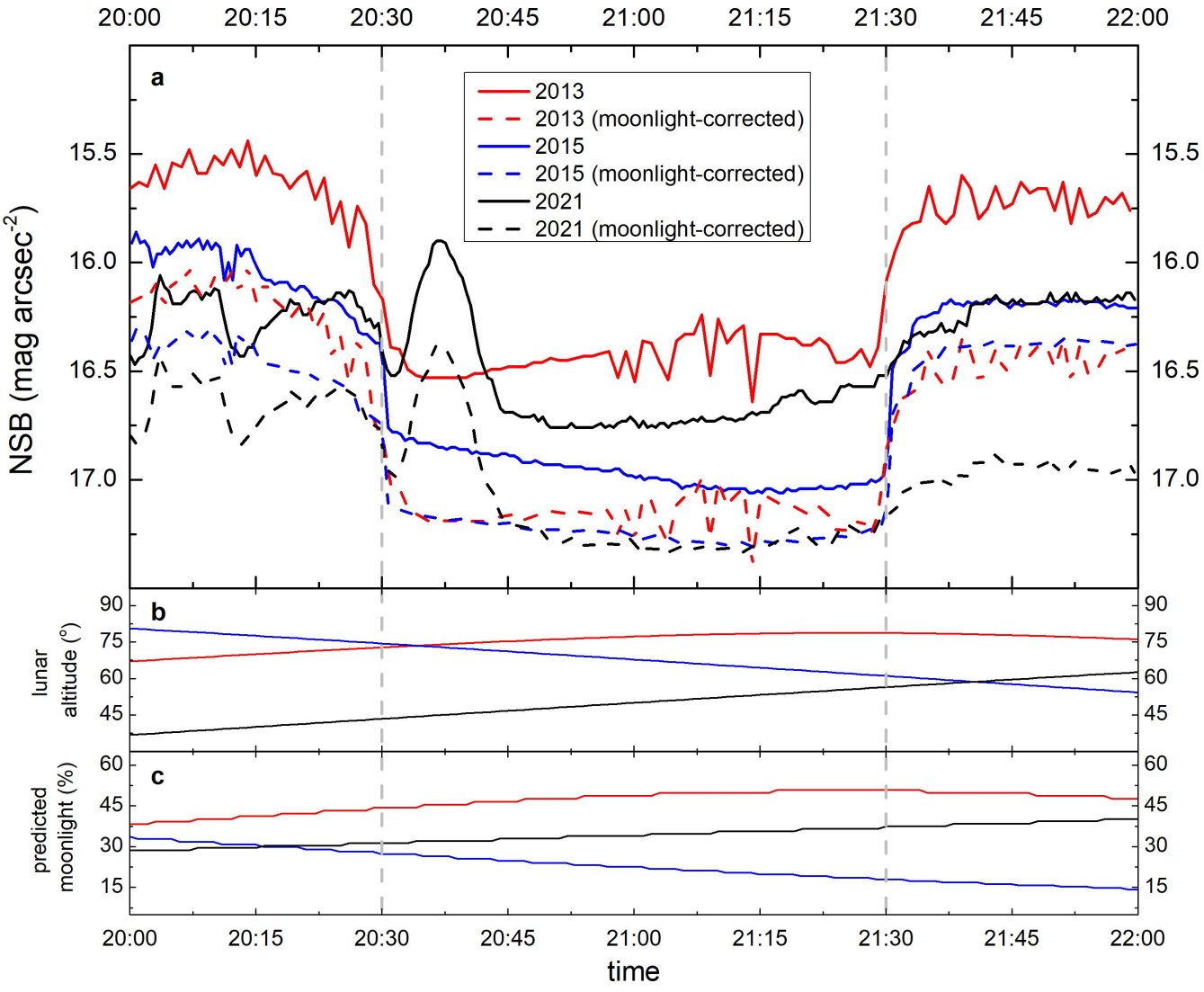

Figure 7. The NSB light curves before and after moonlight corrections during Earth Hours 2013, 2015 and 2021 are presented as follows: (**a**) The original NSB light curves are shown as solid curves, while the moonlight-corrected curves are represented as dashed curves. Vertical dashed lines indicate the start and end of the lights-out period; (**b**) Lunar altitude variations in 2013 (red), 2015 (blue) and 2021 (black), calculated with ALCYONE EPHEMERIS version 4.3; (**c**) Predicted moonlight contributions for 2013 (red), 2015 (blue) and 2021 (black) (see Methods). Note that the light curves for 2013 and 2015 have been corrected for the shielding on the sensor's housing (Supplementary Note 6).